Збірник праць Інституту математики НАН України 2014, т. 11, № 4, 457–471

УДК 532.595

The vortex-induced damping in the moonpool problem *

A.N. Timokha

Institute of Mathematics of NASU of Ukraine, Kiev, Ukraine;
atimokha@gmail.com

На підставі подібності між вертикальними коливаннями рідини в двовимірному вертикальному мунпулі та коливними течіями крізь отвір перфорованої пластини запропоновано аналітичну модифікацію лінійної гідродинамічної моделі ідеальної течії, яка враховує дисипацію внаслідок розділення рухів рідини навколо кромок мунпула. У наслідок цього теоретичні результати кількісно відповідають раніше проведеним експериментальним тестам та розрахункам за нелінійними моделями в'язкої рідини.

Используя подобие между вертикальными колебаниями жидкости в двумерном вертикальном мунпуле и колебательными течениями через отверстие перфорированного экрана, предлагается аналитическая модификация линейной гидродинамической модели идеальной жидкости, которая учитывает диссипацию вследствие разделения течений жидкости около кромок мунпула. Это делает теоретические результаты количественно соответствующими ранее выполненным экспериментальным тестам и расчетам с использованием нелинейных моделей вязкой жидкости.

1. Introduction

Three- and two-dimensional piston-type resonant sloshing in a moonpoon (vertical opening through the deck and hull of ships or barges) was extensively studied from fundamental and practical points of view, e.g., in [2,3,6,12,13,15]. Perhaps, due to the trapped waves problem (reviews

* This work has been carried out at the Centre of Autonomous Marine Operations and Systems (AMOS). The Norwegian Research Council is aknowledged as the main sponsor of AMOS (Project number 223254–AMOS). In addition, the work was partly supported by the Grants No 0107U002198 and 0113U003270.

can be found in [10,11,14]) clarifying hydrodynamic resonances in moonpools within the framework of the inviscid potential flow model, various potential flow solvers remain a generally accepted tool for describing a resonant sloshing in moonpools (see, recent papers [9,16–18]).

Paper [6] reported model tests and an accurate linear inviscid potential flow solver (which handles singular behaviour at sharp edges) for a two-dimensional rectangular moonpool. Focusing on this simple geometric shape, [6] pursued addressing a fundamental question – to what extend is the inviscid potential flow model applicable for quantifying the resonance frequencies and the forced piston-type liquid motion? Conclusions were that the resonance frequencies are theoretically well predicted but there are discrepancies between theoretical and experimental data for the forced resonant steady-state wave elevations in the moonpool opening. The discrepancies could be explained by a flow separation at lower moonpool edges, a phenomenon, which was experimentally observed in [8,13].

Experimental results from [6] were further re-analysed in [2]. It was found out that reflection of outgoing waves at the wave basin walls was not negligible and may matter for the discrepancies. Paper [4] has done additional model tests with the same input parameters for which, believable, the reflection effect is minimal. In addition, papers [2,4] developed two different viscous solvers modelling the local flow at the lower moonpool edges and, thereby, obtained a good agreement with the experimental steady-state resonant response. This means that the moonpool problem requires either creating appropriate viscous solvers or modifying the existing inviscid potential flow model which should include the vortex-induced damping effect.

Working on sloshing in a screen-equipped tank, paper [5] faced the same need in modifying the multimodal method which is a kind of an analytical inviscid potential flow solver. Handbook [1] lists formulas and tables for coefficients in the pressure discharge condition due to flow separation on the screen. The coefficients can be effectively computed for various screen patterns as functions of the screen solidity ratio and, if needed, the Keulegan-Carpenter number. Discovering a similarity between the piston-type sloshing in a two-dimensional rectangular moonpool and oscillatory flows through a cell of a slat-type screen, the present paper shows how to account for the vortex-induced damping in the resonant moonpool problem. The necessary components are (a) a potential flow solver, (b) the pressure discharge condition following from that for

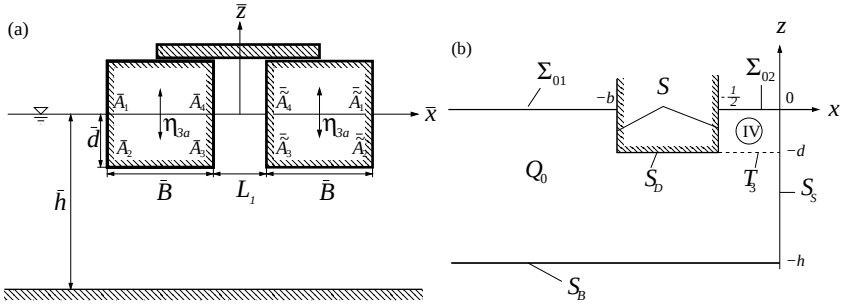

Fig 1. A sketch of dimensional moonpool problem (panel a) and the left part of the L_1-normalised symmetric liquid domain as considered in [6] and suggested in the quasi-linear statement (6)–(10), panel (b).

a screen whose cells has the same shape as the moonpool opening, and (c) an estimate of an artificial (fictional) solidity ratio which can be obtained by inverting Molin's formula [12]. Mathematically, adopting (a) and (b) leads to an extra nonlinear term in the dynamic boundary condition on the 'inner' free surface (in the moonpool opening) within the framework of a linear inviscid potential flow model. The coefficient in front of this nonlinear term depends on the resonant frequency which should be *a priori* computed. We illustrate how to solve the modified problem with using the equivalent linearisation and the domain decomposition scheme from [6]. The numerical results are well supported by earlier experiments and the nonlinear steady-state viscous solutions from [2, 4].

2. Statement

We consider two-dimensional $O\bar{z}$-symmetric *steady-state surface waves* excited by small-amplitude vertical harmonic motions of two rigidly-connected rectangular hulls, $\eta_3(t) = \eta_{3a}\sin(\sigma t)$, in the finite water depth as shown in Fig. 1 a. At a certain forcing frequency σ_*, a resonant vertical piston-type sloshing occurs between the hulls, $-\frac{1}{2}L_1 < x < \frac{1}{2}L_1$. Paper [6] studied the potential inviscid liquid motions in a linear nondimensional statement assuming L_1 is the characteristic size and $1/\sigma$ is the characteristic time. This implies the nondimensional variables

$$x = \bar{x}/L_1; \quad z = \bar{z}/L_1; \quad t = \sigma\bar{t}; \quad \Lambda = \sigma^2 L_1/g, \quad \epsilon = \eta_{3a}/L_1 \ll 1, \qquad (1)$$

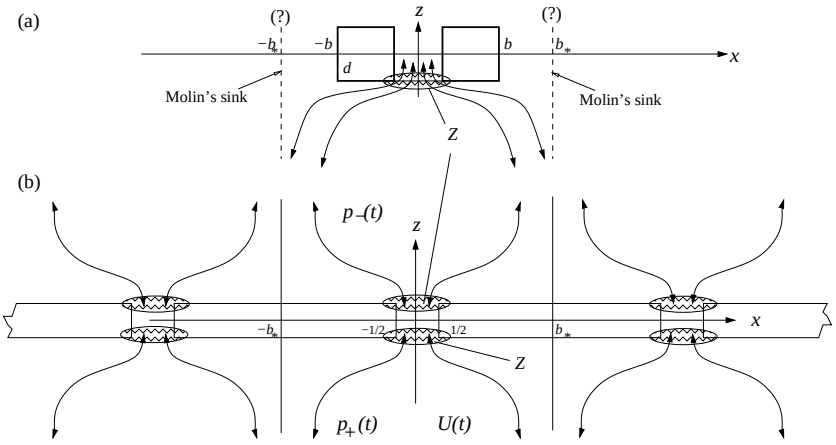

Fig 2. Panel (a) schematically illustrates streamlines associated with the steady-state resonant piston-type sloshing in a rectangular moonpool ($z < 0$) with a finite water depth. A nondimensional view where the slot length is the characteristic size. The vortices are assumed localised in zone Z between two edges so that a pressure discharge occurs along the line connecting the edges. The introduced vertical lines $x = \pm b_*$ [approximately] bound fluid particles which determine an up-and-down flow through the moonpool opening, i.e. these are the bounds of a global stream tube. Estimating b_* is possible by inverting Molin's formula. Panel (b) schematically depicts an oscillatory inviscid potential flow through a cell of a slat-type screen with a uniform approach velocity $U(t)$. Fluid particles do not cross the vertical lines $x = \pm b_*$ which determine a global stream tube for a chosen cell. Points $\pm b_*$ are normally at the slat middle for a uniform screen geometry but their position may change when the slat/slot lengths slightly vary away from the considered cell. The actual screen solidity ratio at O can be approximated as $Sn = (2b_* - 1)/(2b_*)$. In contract to the case (a), the vortices are localized at two (upper and lower) zones Z so that the pressure discharge at the cell is twice larger than at the moonpool opening.

where g is the gravity acceleration. As a consequence, the distance between the rectangular bodies and the Oz-axis (symmetry-axis) becomes equal to $\frac{1}{2}$, the nondimensional water depth is $h = \bar{h}/L_1$, the scaled dimensions of the stationary immersed rectangular body are $d = \bar{d}/L_1$ in vertical (draft) and $B = \bar{B}/L_1 = \bar{b}/L_1 - \frac{1}{2}$ in horizontal direction, respectively. The left normalised liquid domain is shown in Fig. 1 b.

Paper [6] showed that an inviscid potential flow solution accurately predicts the resonant frequency σ_* (or the nondimensional value $\Lambda_* = \sigma_*^2 L_1/g$ by (1)) of the piston-type sloshing in a rectangular moonpool. An inviscid hydrodynamic model is also efficient in computing the resonant sloshing frequencies in a screen-equipped tank [7]. The inviscid potential liquid motions define in both cases an ambient flow for estimating an overall damping due to the vortex shedding at the lower sharp edges.

In our analysis, the rigid block draft d is finite so that one can assume that the vortices are localised in a zone Z between the edges as depicted in Fig. 2 (a). The zone confines the transmission line T_3 separating the inner liquid domain IV and outer liquid in Fig. 1 (b). Fig. 2 (b) compares inviscid potential flow expectations for a slotted screen with those for the piston-type sloshing in a rectangular moonpool. An important fact is that the liquid flow beneath the rigid rectangular hulls has normally a nonzero horizontal component. This means that the global stream tube for the piston-type sloshing flow inside and beneath the moonpool opening has bounds far from the rigid hulls. The same conclusion comes from analysis [12] which assumes a "frozen" external free surface but poses two sinks with abscissas $\pm b_*, b_* > b$ to compute the resonant frequency σ_*. As matter of fact, the Molin theory approximately defines the streamtube bounds. We accept the Molin prediction. Finding the Molin sinks position implies inverting his nondimensional formula

$$b_* = 2\exp\left((\Lambda_*^{-1} - d)\pi - \tfrac{3}{2}\right), \tag{2}$$

where Λ_* should be *a priori* computed by using an inviscid potential flow solver.

For the screen-affected sloshing, paper [5] needed the following two *input parameters* coming from the inviscid potential flow solution: (i) the spatially-averaged (uniform) velocity $U(t)$ associated with the liquid flux through the screen openings, it defines the so-called approach velocity and (ii) the solidity ratio Sn which is a geometric characteristics of the chosen screen. When the slotted screen consists of slots with slightly varying lengths, considering a single screen cell helps estimating the solidity ratio via the formula $Sn = (2b_* - 1)/(2b_*)$ where $-b_* < x < b_*$. For a uniformly slotted screen, points $\pm b_*$ lay in the slats middles. As for estimating $U(t)$, if $u_0(t)$ is the mean x-averaged relative velocity through the chosen cell opening, the approach velocity within the streamtube $-b_* < x < b_*$ can be found via $U(t) = u_0(t)/(2b_*)$. The *output* in the screen-affected sloshing governs a spatially-averaged pressure jump between upper and

lower liquid subdomains introducing an additional (to the hydrodynamic pressure within the framework of the inviscid potential flow solution) pressures $\bar{p}_-(t)$ and $\bar{p}_+(t)$ as shown in Fig. 2. The dimensional pressure discharge condition is

$$\Delta\bar{p} = \bar{p}_+(t) - \bar{p}_-(t) = \tfrac{1}{2}\rho K\bar{U}(t)|\bar{U}(t)| \tag{3}$$

where ρ is the liquid density and the nondimensional pressure drop (discharge) coefficient K should be found from experiments as a function of Sn and, generally, the Keulegan–Carpenter number. Paper [5] successfully employed the following formula

$$K = K(Sn) = \left(\frac{1}{C_0(1-Sn)} - 1\right)^2,\ C_0 = 0.405\exp(-\pi Sn) + 0.595, \tag{4}$$

which assumes that K does not depend on the Keulegan-Carpenter number.

Hence, employing a certain potential flow solver can compute Λ_* and approximate b_* by (2) which gives an artificial (fictional) solidity ratio $Sn = (2b_* - 1)/(2b_*)$ for the piston-type resonant sloshing in a rectangular moonpool. The same solver can be adopted to estimate the water flux through the opening and, therefore, as explained above, one can analytically express $U(t)$ via an integral over the vertical derivative of the velocity potential. Remembering (3) and (4) for the slotted screen hydrodynamics, we can estimate the spatially averaged pressure drop in zone Z (projected on T_3) as

$$\begin{aligned} \Delta p &= \tfrac{1}{16}\Lambda\left((C_0(b_*))^{-1} - (2b_*)^{-1}\right)^2 u_0(t)|u_0(t)|, \\ C_0(b_*) &= 0.405\exp\left(-\pi(2b_*)^{-1}\right) + 0.595, \end{aligned} \tag{5}$$

where $u_0(t)$ is the nondimensional x-averaged vertical velocity of the piston-type sloshing in the opening $(-\frac{1}{2}, \frac{1}{2})$; b_* is computed by (2).

Let us modify the linear inviscid potential flow statement due to the pressure discharge (5) through T_3 (see, Fig. 1 b). As in [6], we introduce the nondimensional velocity potential $\psi(x, z, t)$ and focus on the left symmetric mean liquid domain Q_0. The velocity potential is assumed be continuous together with its derivatives except on T_3 where it possesses the t-depending jump, $\psi_{IV}(y, z, t) = \psi(y, z, t) + \Delta p(t)$. The following equation and boundary conditions with respect to $\psi(x, z, t)$ are

taken from [6]:

$$\nabla^2\psi = 0 \text{ in } Q_0,\ \frac{\partial\psi}{\partial n} = 0 \text{ on } S_B + S + S_S,\ \frac{\partial\psi}{\partial z} = \epsilon\sin t \text{ on } S_D, \quad (6)$$

$$\Lambda\frac{\partial^2\psi}{\partial t^2} + \frac{\partial\psi}{\partial z} = 0 \quad \text{on} \quad \Sigma_{01}, \quad (7)$$

where Σ_{01} is the unperturbed free surface outside the moonpool opening, S is the mean wetted vertical walls of the stationary rectangle, S_B is the horizontal seabed, S_D is the bottom of the rectangular body, S_S is the artificial vertical wall caused by the Oz-symmetry and n is the outer normal to the fluid boundary. The linear kinematic and dynamic conditions on the mean free surface Σ_{02} *inside* the opening take, accounting for the pressure discharge (5) on T_3, the following form

$$\frac{\partial\psi}{\partial z} = \frac{\partial f}{\partial t} \text{ and } \Lambda\frac{\partial\psi}{\partial t} + f = \tfrac{1}{16}\Lambda\left((C_0(b_*))^{-1} - (2b_*)^{-1}\right)u_0(t)|u_0(t)|, \quad (8)$$

where $z = f(x,t)$ defines the free surface elevation and the mean relative velocity on T_3 (see, Fig. 1 b)

$$u_0(t) = 2\int_{-1/2}^{0}\frac{\partial\psi}{\partial z}(x,-d,t)\mathrm{d}x - \epsilon\sin t. \quad (9)$$

Finally, we need a condition at infinity ($x \to -\infty$) for outgoing waves and should remember that the analysis is restricted to the steady-state solutions, i.e.

$$\psi \sim F(\mathcal{K}x + t, z) \quad \text{as} \quad x \to -\infty; \quad \psi(x,z,t+2\pi) \equiv \psi(x,z,t), \quad (10)$$

where $\mathcal{K}$ is the wave number of the outgoing wave.

The problem (6)–(10) is a quasi-linear boundary value problem with a single nonlinear integral term in the dynamic boundary condition (8). Specifically, solving (6)–(10) implies *a priori* finding the nondimensional resonant frequency Λ_* and b_* by (2) from the linearized statement. Appropriate procedure is described in [6]. Furthermore, due to the nonlinearity, the steady-state (periodic) solution can be presented by a Fourier series where higher harmonics may matter, but, generally speaking, adopting the linear free-surface condition suggests the $\cos t$ and $\sin t$ components are dominants. These components can be found based on slightly modified solver from [6]. The obtained numerical results will be compared with already-published experimental measurements and viscous solutions in the next section.

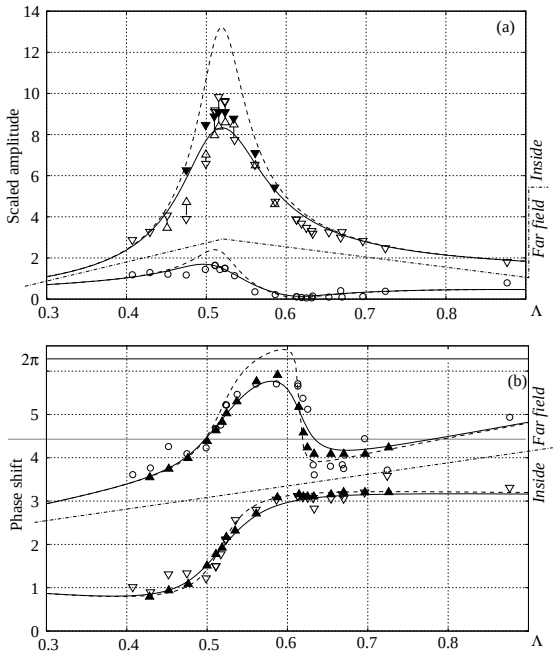

Fig 3. Experimental case 1 from [6] ($B = 1, d = 1$, and $h = 5.72222$). Theoretical and experimental maximum wave elevations of the piston-type sloshing ('Inside') and the maximum wave elevations at $x = w11 = 3.88889$ ('Far field') are scaled by the forcing amplitude in panel (a). Panel (b) present the corresponding phase shifts relative to the input sinusoidal motions of the hulls. The nondimensional forcing amplitude $\epsilon = 0.013889$. The experimental data are from [6]: $\triangle$ corresponds to the maximum steady-state wave elevations inside the moonpool opening ('Inside') (a) and the corresponding phase shifts (b); $\circ$ denotes the measured maximum wave elevation and phase shift at $x = 3.88889$ ('Far field'), and $\triangledown$ marks the measured maximum elevations inside the opening filtered against the reflection effect of the outgoing wave (done by in [2]). The dashed lines are taken from [6] and denote the inviscid potential flow prediction. The solid lines present our computations accounting for the $\sin t$ and $\cos t$ harmonics. Other numerical results are marked by solid triangles.

3. Numerical steady-state solution

Comparisons of our dominant harmonic approximation (solid lines) with experimental steady-state measurements (empty symbols), and nonlinear

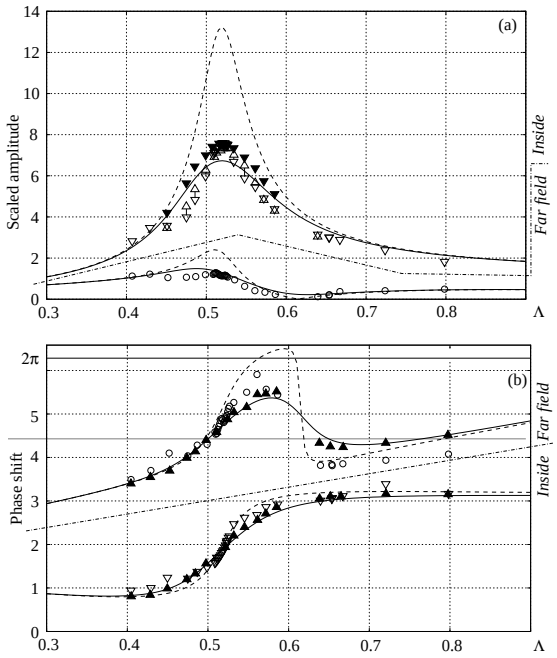

Fig 4. The same as in Fig. 3 but for $\epsilon = 0.027778$.

viscous simulations (solid symbols) are presented in Figs. 3–8. In additional, the dashed lines denote numerical results from [6] obtained by the linear inviscid potential flow solver. Focus is on the maximum wave elevations inside the moonpool opening, the maximum wave elevations far from the hulls (at the control point $x = w11$), and the corresponding phase shifts (with respect to the $\sin t$ input signal for the forced motions of the hulls). More details on the experimental setup can be found in [4, 6]. Papers [2, 4] also give an extended description of the employed viscous solvers.

Figs. 3 and 4 present comparison results for the experimental case 1 of [6] where, under the same input geometric parameters, two different forcing amplitudes were tested. The extended caption explains the adopted notations. One must note that the measured maximum wave elevation inside the moonpool opening is, according to [2], affected by the outgoing waves reflection from a wall of the experimental wave basin.

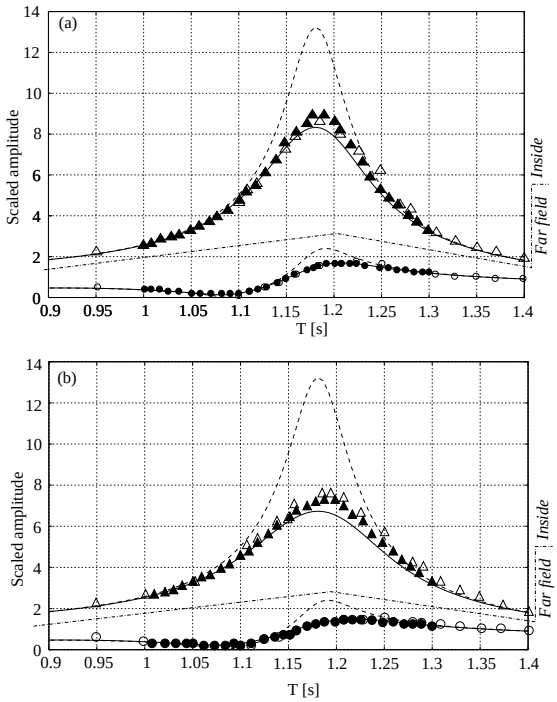

Fig 5. The same as in Fig. 3 (a,c) but in comparison with experiments reported in [4] (empty symbols). As in the original experimental publication, the amplitude and phase shift results are given versus the dimensional forcing period T [s]. The solid symbols ▲ (maximum wave elevation) and • (phase shift) show the numerical results from [4] obtained by employing a viscous solver for the liquid domain beneath of the hulls and inside the moonpool opening.

Other measurements, namely, the maximum wave elevation at $w11$ and the phase shifts were almost not influenced by the reflection. Thus, along with symbols △ illustrating the actual measurements of the maximum wave elevation in the moonpool opening, we introduce inverted symbols ▽ which denote a filtered output signal that are, believable, not affected by the reflection. What we see from the figure is that our theoretical results are now in satisfactory agreement with both the filtered measurements of the maximum wave elevations and with other measured outputs.

Paper [2] conducted nonlinear simulations accounting for the vortex

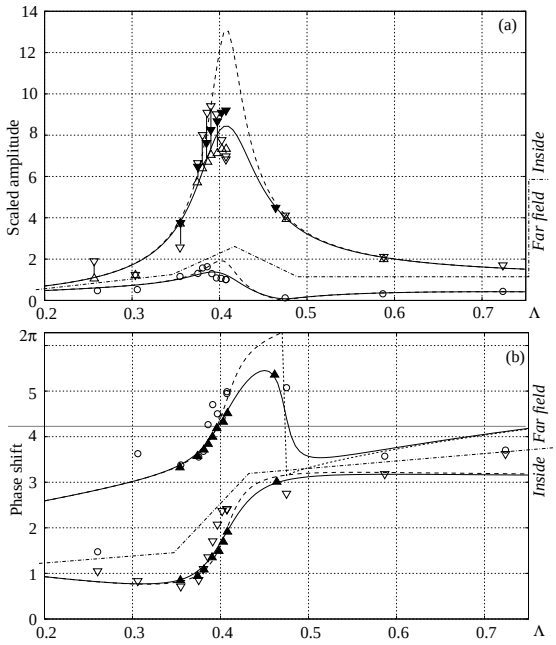

Fig 6. The same as in Fig. 3 but for the experimental case 2 from [6] ($d = 1.5$).

shedding at the sharp lower edges of the rigid hulls. Their numerical results are shown by solid triangles: symbols ▼ denote numerical maximum wave elevations inside the moonpool opening and symbols ▲ mark numerical results for the phase shifts. Again, we see a good agreement with our theory (compare the solid symbols and the solid lines) but our theoretical data are slightly lower of those following from simulations in [2]. A difference may be due to the fact that out theoretical values account only for the $\sin t$ and $\cos t$ components, but higher harmonics, e.g., $\cos 3t$ and $\sin 3t$, yielded by the $(|\cdot|\cdot)$-nonlinearity can matter in a certain forcing frequency range.

Paper [4] describes additional model tests with the same input parameter as in case 1. These model tests pursued minimizing the abovementioned reflection effect. They also proposed a domain decomposition method which suggests a viscous solver for the fluid domain beneath and inside of the rectangular moonpool. We compare our theoretical output (solid lines), the inviscid potential flow solution (dashed lines) and

these additional experimental and numerical results in Fig. 5. Again, we see that our single harmonics approximation of the steady-state solution gives slightly lower values for the maximum wave elevations in the moonpool opening with respect to those in [4]. However, agreement looks satisfactory accounting for the hydrodynamic model simplicity and many extra factors which may contribute the maximum wave elevation but are ignored by our theory. An example is the aforementioned higher harmonics.

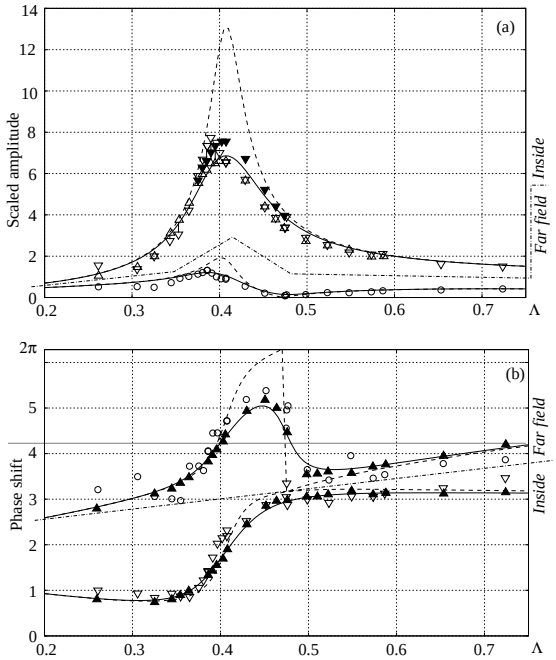

Fig 7. The same as in Fig. 4 but for the experimental case 2 from [6] ($d = 1.5$).

Experimental cases 2 and 3 from [6] are analyzed in Figs. 6, 7 and 8. Again, our approximation is in a satisfactory agreement with model tests (filtered against the outgoing wave reflection) and nonlinear simulations in [2]. This is especially for simulations in case 3.

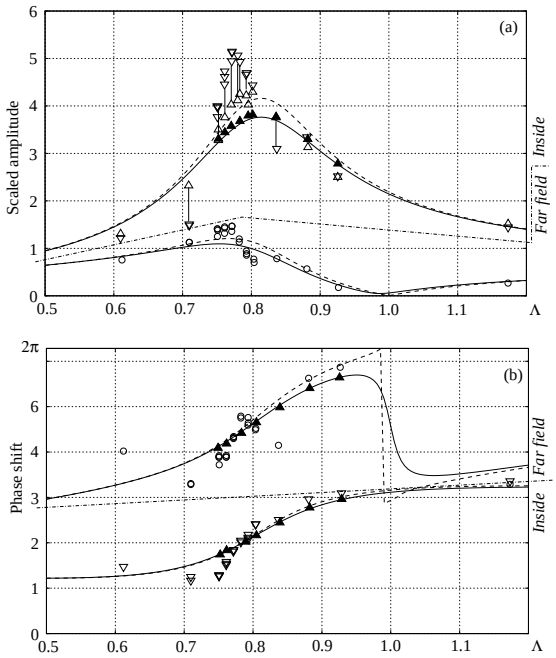

Fig 8. The same as in Fig. 3 but for the experimental case 3 ($B = 1, d = 0.5, h = 2.86111, \epsilon = 0.006944$ and $w11 = 1.94444$).

4. Conclusions

Describing the piston-type resonant sloshing in a moonpool traditionally involves inviscid potential flow solvers (see, [9, 16–18], and reference therein) which give an accurate prediction of the resonant frequencies but may cause differences from experimental measurements in quantifying the resonant response amplitudes. A reason is the vortex-induced damping at the lower moonpool edges visualized in experiments [8, 13]. A straightforward way for getting an accurate theoretical prediction consists of using viscous solvers, at least, for the liquid domain beneath the hulls and inside the moonpool opening. Studies [2, 4] (two-dimensional moonpool) followed it.

We discover a similarity between the inviscid potential flows in a rectangular moonpool and those at a cell of a slat-type screen. An extra drag [pressure drop] force term counteracting the piston-type liquid motions

inside the moonpool opening was derived. As a consequence, we have got an extra nonlinear quantity in the dynamic boundary condition on the inner (with respect to the moonpool) free surface. The quantity contains an auxiliary (fictional) solidity ratio coming from the screen problems. For rectangular two-dimensional moonpool, this ratio can be estimated by inverting Molin's formula for the resonant frequency assuming that the frequency is found by using another numerical method, e.g., [6]. Comparing the numerical results with experimental data from Part 1, other experimental and numerical results in [2,4] (obtained by adopting viscous solvers) showed a satisfactory agreement. This is even though our computations are based on equivalent linearization and account only for the first harmonics in a Fourier solution of the derived quasi-linear boundary problem.

Even though employing an inviscid potential flow solver from [6] makes it possible to get results only for the two-dimensional rectangular moonpool, we see a perspective of using the proposed analytical approach for other moonpool shapes facilitated by existing potential flow solvers. First, there is a variety of formulas for estimating the pressure drop [drag force] coefficients for screens which, hopefully, may cover all practical moonpool shapes. This implies that formula (4) should change. Secondly, [15] discussed generalizations of Molin's formula [12] for different two- and three-dimensional moonpools. This implies that one can estimate the fictional solidity ratio Sn.

[1] *Blevins R.* Applied Fluid Dynamics.– Malabar, FL: Krieger Publishing Company, 1992.

[2] *Kristiansen T., Faltinsen O.* Application of a vortex tracking method to the piston-like behaviour in a semi-entrained vertical gap // Appl. Ocean Res.– 2008.– **30**.– P. 1–18.

[3] *Kristiansen T., Faltinsen O.* A two-dimensional numerical and experimental study of resonant coupled ship and piston-mode motion // Ibid.– 2010.– **32**.– P. 158–176.

[4] *Kristiansen T., Faltinsen O.* Gap resonance analyzed by a new domain-decomposition method combining potential and viscous flow DRAFT // Ibid.– 2012.– **34**.– P. 198–208.

[5] *Faltinsen O., Firoozkoohi R., Timokha A.* Steady-state liquid sloshing in a rectangular tank with a slat-type screen in the middle: quasi-linear modal analysis and experiments // Phys. Fluids.– 2011.– **23**, Art. No 042101.

[6] *Faltinsen O., Rognebakke O., Timokha A.* Two-dimensional resonant piston-like sloshing in a moonpool // J. Fluid Mech.– 2007.– **575**.– P. 359–397.

[7] *Faltinsen O., Timokha A.* Natural sloshing frequencies and modes in a rectangular tank with a slat-type screen // J. Sound Vibr.– 2011.– **330**.– P. 1490–1503.

[8] *Fukuda K.* Behaviour of water in vetical well with bottom opening of ship, and its effect on ship motions // J. Soc. Naval Archit. Jap.– 1977.– **141**.– P. 107–122.

[9] *Liu Y., Li H.-J.* A new semi-analytical solution for gap resonance between twin rectangular boxes // Proc. Institution of Mechanical Engineers, Part M: J. Eng. Maritime Env.– 2014.– **228**.– P. 3–16.

[10] *McIver P., McIver M.* Motion trapping structures in the three-dimensional water-wave problem // J. Eng. Math.– 2007.– **58**.– P. 67–75.

[11] *McIver P., Newman J.* Trapping structures in the three-dimensional water-wave problem // J. Fluid Mech.– 2003.– **484**.– P. 283–301.

[12] *Molin B.* On the piston and sloshing modes in moonpools // Ibid.– 2001.– **430**.– P. 27-50.

[13] *Molin B., Remy F., Kimmoun O., Stassen Y.* Experimental study of the wave propagation and decay in a channel through a rigid ice-sheet // Appl. Ocean Res.– 2002.– **24**.– P. 5–20.

[14] *Newman J.* Trapping of water waves by moored bodies // J. Eng. Math.– 2008.– **62**.– P. 303–314.

[15] *Sajjan S., Surendran S.* Effect of Pretension on Moored Ship Response International // J. Ocean Syst. Eng.– 2013.– **3**.– P. 175–187.

[16] *Zhang X., Bandyk P.* On two-dimensional moonpool resonance for twin bodies in a two-layer fluid // Appl. Ocean Res.– 2013.– **40**.– P. 1–13.

[17] *Zhou H., Wu G., Zhang H.* Wave radiation and diffraction by a two-dimensional floating rectangular body with an opening in its bottom // J. Eng. Math.– 2013.– **83**.– P. 1–22.

[18] *Zhou H.-W.* Radiation and diffraction analysis of a cylindrical body with a moon pool // *J. Hydrodynamics*.– 2013.– **25**.– P. 196–204.